

RESEARCH ARTICLE | DECEMBER 10 2024

Time transfer and clock synchronization with ghost frequency comb

Binod Joshi   ; Thomas A. Smith  ; Yanhua Shih 

 Check for updates

Appl. Phys. Lett. 125, 241105 (2024)

<https://doi.org/10.1063/5.0243508>



Articles You May Be Interested In

Selection and amplification of a single optical frequency comb mode for laser cooling of the strontium atoms in an optical clock

Appl. Phys. Lett. (October 2015)

Long distance measurement up to 1.2 km by electro-optic dual-comb interferometry

Appl. Phys. Lett. (December 2017)

Active laser ranging with frequency transfer using frequency comb

Appl. Phys. Lett. (May 2016)

28 February 2025 15:53:11



Nanotechnology & Materials Science



Optics & Photonics



Impedance Analysis



Scanning Probe Microscopy



Sensors



Failure Analysis & Semiconductors



Unlock the Full Spectrum. From DC to 8.5 GHz.

Your Application. Measured.

[Find out more](#)



Time transfer and clock synchronization with ghost frequency comb

Cite as: Appl. Phys. Lett. **125**, 241105 (2024); doi: [10.1063/5.0243508](https://doi.org/10.1063/5.0243508)

Submitted: 11 October 2024 · Accepted: 26 November 2024 ·

Published Online: 10 December 2024






View Online



Export Citation



CrossMark

Binod Joshi,^{1,a)}  Thomas A. Smith,²  and Yanhua Shih¹ 

AFFILIATIONS

¹Department of Physics, University of Maryland Baltimore County, Baltimore, Maryland 21250, USA

²Quantum Research and Applications Branch, Naval Air Warfare Center, Patuxent River, Maryland 20670, USA

^{a)} Author to whom correspondence should be addressed: binodj1@umbc.edu

ABSTRACT

We report an experimental demonstration of a time transfer and distant clock synchronization scheme based on what we have labeled as a ghost frequency comb, observed from the nonlocal correlation measurements of a laser beam. Unlike a conventional frequency comb, the laser beam used in this work does not consist of a pulse train but instead it is in a continuous-wave operation. The laser beam, consisting of half a million longitudinal cavity modes from a fiber ring laser, is split into two beams, each sent to a distant observer. In their local measurements, both observers observe constant intensity with no pulse structure present. Surprisingly, a pulse train of comb-like, ultra-narrow peaks is observed from their nonlocal correlation function measurement. This observation makes an important contribution to the field of precision spectroscopy, as we show in optical correlation-based nonlocal timing and positioning.

Published under an exclusive license by AIP Publishing. <https://doi.org/10.1063/5.0243508>

Since the development of frequency combs led by John Hall and Theodor Hänsch, researchers have developed a wide array of practical applications for these light sources.^{1–6} The precise structure of a frequency-time comb enables precision spectroscopy that makes it possible to measure time and frequency of light more accurately than ever before.^{7,8} Frequency combs have been demonstrated to significantly improve clock synchronization and light detection and ranging (LiDAR), among other applications.^{9–15} In this Letter, we report a recent experimental application of a different type of frequency-time comb, which we label as a ghost frequency comb (GFC). A laser beam with many longitudinal modes was operated in the continuous-wave (CW) mode with no pulse structure present. Even though no pulses could be measured by a photodetector, surprisingly, a frequency-time comb was observed from the nonlocal correlation measurement between two point-like, independent photodetectors.¹⁶ The fundamental question on how a coherent CW laser beam produces nontrivial intensity correlation like thermal light has been addressed and studied recently,¹⁷ but without further discussion on any potential applications. We anticipate that the ghost frequency comb introduced in this Letter will be similarly useful for many applications traditional frequency combs are utilized for, but with the added intrigue of nonlocal effects. Here, we present a proof-of-concept for one potential application: nonlocal time transfer.^{18,19}

Traditional frequency combs can be generated by different methods—a common technique being mode-locked lasers.²⁰ Such lasers are

designed to generate light from a certain number of evenly spaced longitudinal cavity modes resulting in a spectrum that resembles a comb-like structure. Then the mode-locking mechanism ensures that the light waves from each of the longitudinal cavity modes are coherently superimposed to produce a succession of well-defined pulses that are evenly spaced in time, thus resulting in a comb-like laser beam (along the direction of beam propagation).

The laser used in the presented experiment is a standard fiber ring laser that consists of a large number of evenly spaced longitudinal cavity modes like that of a frequency comb; however, it does *not* have any mode-locking mechanism. Therefore, unlike a traditional frequency comb, the laser beam does not consist of a pulse train but instead it is a continuous wave. As expected, an individual detector simply measures a constant signal; however, interestingly, the nonlocal correlation measurement between a pair of individual distant detectors produces a set of well-defined, comb-like, ultra-narrow peaks, namely a ghost “pulse” train.

Correlation measurements with light, like those done to reveal the ghost frequency comb reported here, were first conducted in the 1950s by Hanbury Brown and Twiss (HBT) using chaotic light sources such as stars and lamps.^{21,22} Since then, and with the development of lasers and entangled photon sources, optical correlations have been implemented in a wide range of setups. The label “ghost” was given by the physics community in 1995 to the surprising experimental observations of *nonlocal* correlations (coincidence counts) of entangled

photon pairs.^{23,24} In fact, this label for nonlocal correlations is not limited to entangled states—in HBT-type intensity correlation measurements, similar “ghosts” from thermal states have been successfully observed, except a lower contrast of 50%.^{25–27} Many other findings have utilized the name ghost to distinguish them from their traditional counterparts, such as *ghost imaging*, *ghost diffraction*, and *ghost spectroscopy*.^{28–30} As with those measurements, we have found that the GFC reported here accurately matches the theoretical calculations of the second-order coherence function, based on Glauber’s quantum theory of optical coherence^{31,32} as well as an electric field description of the multi-longitudinal-mode fiber laser, as will be shown later in this report. As ghost measurements often involve entanglement, and similar correlations from spontaneous parametric downconversion (SPDC) have been reported previously,^{33–35} it is worth emphasizing that the presented work does *not* utilize any entanglement. Our work is based on bright light of TEM₀₀ laser beam allowing it to be sent to longer distance (diffraction limited propagation) for nonlocal correlation measurement and, unlike in SPDC sources, does not require photon counting methods.

Our experimental setup is demonstrated in Fig. 1. To generate a GFC, a laboratory-assembled CW fiber ring laser was used, which consisted of a pump laser beam, an 8 m erbium-doped fiber amplifier (EDFA), and an 11.7 km single-mode optical fiber ring cavity. The EDFA in combination with the 11.7 km ring cavity generated approximately half a million evenly spaced longitudinal cavity modes all in the TEM₀₀ transverse profile. As typical, the ring laser produced two beams propagating in opposite directions around the cavity, but only one output was used for this demonstration. Many measurements were done in the range 1.4–2.8 mW of the pump power, which was clearly above the threshold pump power of approximately 0.38 mW needed for lasing. The pump power was also kept sufficiently low to avoid any unwanted passive mode-locking, thus preventing any pulse-like structure. The power spectrum recorded by an optical spectrum analyzer (OSA) measured a full width at half maximum (FWHM) bandwidth of $\Delta\lambda \simeq 0.07$ nm ($\Delta f \simeq 8.6$ GHz) centered in the range of 1562–1563 nm, which is within the conventional band (C-band) optical fiber transmission window. For this ring cavity with a length of 11.7 km, the theoretically expected value of mode separation

is $\nu_b = 17\,464.26$ Hz.³⁶ Using the laser bandwidth of 8.6 GHz measured by the OSA, this gives a calculated value of $N = 492\,554$, which we will approximate simply as $N \simeq 500\,000$. We used the standard C-band optical fibers for which the precise values of the index of refraction and the uncertainties associated with them were unavailable; hence, the value of the refractive index was taken to be 1.468, which is typical for the C-band optical fiber. This introduces a degree of uncertainty into our results (based on the available information, the estimated upper bound of the uncertainty in the theoretical value of ν_b was ± 62.86 Hz); nevertheless, as we show later, our experimental data still find a very close match.

To conduct the measurements, the CW laser beam is passed through a fiber beam splitter and sent to two point-like analog photodetectors, D_1 and D_2 , each of which has a response bandwidth of 5 GHz. The output photocurrents of the photodiodes $i_1(t_1) \propto I_1(t_1)$ and $i_2(t_2) \propto I_2(t_2)$, with their registration times t_1 and t_2 , respectively, are registered by a high speed analog-to-digital converter. The j th event timer on the converter produces a time series of the photodetection events of the j th photodetector D_j , where $j = 1, 2$. Unlike a traditional frequency comb, which produces clear, distinct pulses in the measurement of intensity, the expected value of intensity, $\langle I_j(t_j) \rangle$, for the presented CW laser is a constant. As expected, the measurements of D_1 and D_2 both report constant intensities. To provide the underlying theoretical basis for the experimental observations, we begin by modeling the total electric field incident on detector D_j from N longitudinal modes of a CW laser with discrete, evenly spaced frequencies as

$$E(\tau_j) = \sum_m^N E_m(\tau_j) = \sum_m^N E_0(\omega_m) e^{-i\omega_m \tau_j} e^{i\phi_m}, \quad (1)$$

where m denotes individual longitudinal modes making ω_m and $E_0(\omega_m)$, respectively, the angular frequency and complex amplitude of the m th mode. Here, τ_j is defined as $t_j - r_j/c$, with (r_j, t_j) representing the space-time coordinates of the detector D_j , and c being the propagating speed of light in the medium (in this case, optical fiber). The term ϕ_m represents the random initial phase of the m th mode. We also define the equal spacing of longitudinal modes as the minimum beat frequency, ω_b , such that the frequency of each mode can be

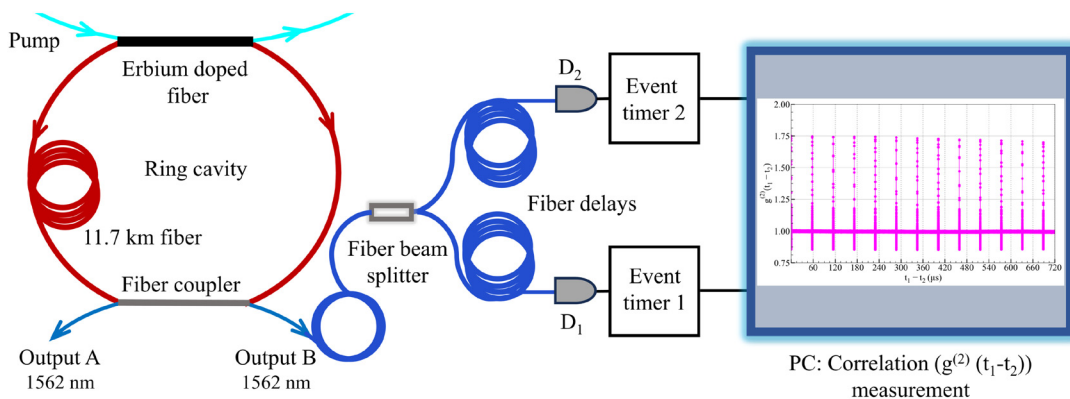


FIG. 1. Schematic setup for experimental demonstration of a ghost frequency comb. Light from a fiber ring laser is directed into a fiber beam splitter. The outputs of the beam splitter pass through fiber optic delays and are fed into two photodetectors D_1 and D_2 . The event timer for each detector produces a time series of the photodetection events of that detector, which can be further analyzed by a computer (PC). The correlation calculation done on these time series reveals a ghost frequency comb, as demonstrated by the miniature of Fig. 2(a) on the PC.

written as $\omega_m = \omega_0 + m\omega_b$, where ω_0 can be considered as a carrier frequency.

The case of independent initial phases of the many cavity modes is distinctly different from a traditional frequency comb, such as a mode-locked laser, for which the initial phases are all *in-phase*, $\phi_m = \phi_0$. In the latter, the coherent superposition of the longitudinal modes results in a clear pulse train in the measured intensity—as expected from a frequency comb. When the phases ϕ_m are all independent and vary randomly, as is the case for the CW laser used in this demonstration, the superposition is incoherent. With this, the intensity measured at detector D_j is written as

$$I(\tau_j) = \sum_{m,n}^N E_m^*(\tau_j) E_n(\tau_j) \\ = \left[\sum_{m=0}^{N-1} E_0^*(\omega_m) e^{im\omega_b\tau_j} e^{-i\phi_m} \right] \left[\sum_{n=0}^{N-1} E_0(\omega_n) e^{-in\omega_b\tau_j} e^{i\phi_n} \right]. \quad (2)$$

We find that when the expectation value, denoted with angled brackets, of the measured intensity is being evaluated, only the terms with $m = n$ survive from the ensemble average, resulting in a constant expectation value of intensity

$$\left\langle \sum_{m=n}^{N-1} E_0^*(\omega_m) E_0(\omega_n) e^{i(m-n)\omega_b\tau_j} e^{-i(\phi_m-\phi_n)} \right\rangle = I_0. \quad (3)$$

The $m \neq n$ terms, which we will label as intensity fluctuations, $\Delta I(\tau_j)$, contain all of the cross terms with the various beat notes between all of the superimposed modes. However, due to the random initial phase relationship between them, the expectation value $\Delta I(\tau_j)$ approaches zero when all possible realizations of the fields are made.

The *ghost frequency comb*, on the other hand, is “uncovered” through the calculated correlation $\langle I(\tau_1)I(\tau_2) \rangle$ from the two independently measured time series. A typically observed GFC is reported in Fig. 2. As discussed earlier, a pulse structure is not achieved with an incoherent superposition when the intensity of the beam is measured with a single photodetector. However, we obtain a different, surprising result with the measurement of second-order (intensity-intensity) correlation between a pair of detectors, D_1 and D_2 ,

$$\langle I(\tau_1)I(\tau_2) \rangle = \langle E^*(\tau_1)E(\tau_1)E^*(\tau_2)E(\tau_2) \rangle \\ = \left\langle \sum_m^N E_m^*(\tau_1) \sum_n^N E_n(\tau_1) \sum_q^N E_q^*(\tau_2) \sum_p^N E_p(\tau_2) \right\rangle. \quad (4)$$

Due to the random relative initial phases between the modes, the only surviving terms are the terms where $m = n$ and $q = p$, and the terms where $m = p$ and $n = q$. So we are left with

$$\langle I(\tau_1)I(\tau_2) \rangle = \sum_m^N E_m^*(\tau_1) E_m(\tau_1) \sum_n^N E_n^*(\tau_2) E_n(\tau_2) \\ + \sum_{m \neq n}^N E_m^*(\tau_1) E_n(\tau_1) E_n^*(\tau_2) E_m(\tau_2) \\ = \sum_{m,n} \left| \frac{1}{\sqrt{2}} [E_m(\tau_1) E_n(\tau_2) + E_n(\tau_1) E_m(\tau_2)] \right|^2 \\ = \langle I(\tau_1) \rangle \langle I(\tau_2) \rangle + \langle \Delta I(\tau_1) \Delta I(\tau_2) \rangle, \quad (5)$$

where we see that the leading terms are simply the product of the mean intensity of each detector (a product of constants), and the end

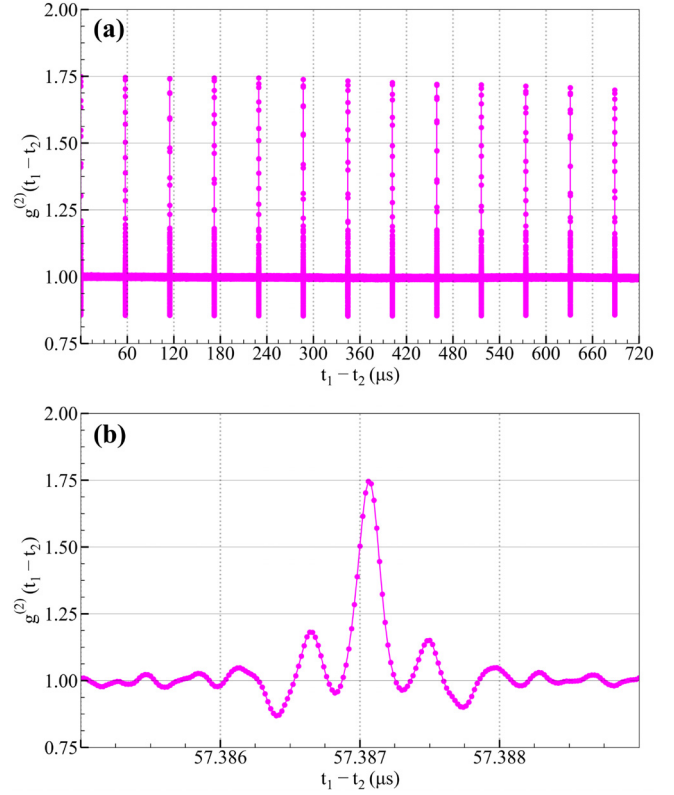


FIG. 2. (a) Typical ghost frequency comb observed from the nonlocal normalized temporal correlation measurements for the setup in Fig. 1. In this measurement, we used two equal length delay lines before D_1 and D_2 . The zero-order ($n = 0$) GFC peak was observed at $\tau_1 - \tau_2 = 0$, or $t_1 - t_2 \approx 0$ when $r_1 \approx r_2$. (b) A closer look at the second GFC peak. A least squares fitting concluded that the GFC has a period of $57\,386.064 \pm 0.001$ ns, equivalent to a beat frequency of $17\,425.8336 \pm 0.0003$ Hz. This value is close to the theoretical estimate of $17\,464.26 \pm 62.86$ Hz. In both plots, the standard error at each value of the correlation is too small to be displayed as an error bar.

terms, the cross-interference terms, are what are known as the intensity fluctuation correlation. Calculating the intensity fluctuation correlation we find that even though the fields are incoherently summed, we are still able to simplify the result due to the cancelation of the initial phases as

$$\langle \Delta I(\tau_1) \Delta I(\tau_2) \rangle = I_0^2 \sum_{m \neq n}^N e^{i\omega_m\tau_1} e^{-i\omega_n\tau_1} e^{i\omega_n\tau_2} e^{-i\omega_m\tau_2} \\ = I_0^2 \left| \sum_m^N e^{i\omega_m\tau} \right|^2, \quad (6)$$

where $\tau \equiv \tau_1 - \tau_2 = (t_1 - t_2) - (r_1 - r_2)/c$, and all constant quantities in the expression have been absorbed into I_0^2 . Using a known exponential sum formula, the result can be calculated as

$$\langle \Delta I(\tau_1) \Delta I(\tau_2) \rangle = I_0^2 \left| \sum_{m=0}^{N-1} e^{im\omega_b\tau} \right|^2 = I_0^2 \frac{\sin^2(N\omega_b\tau/2)}{\sin^2(\omega_b\tau/2)}. \quad (7)$$

It is conventional to normalize the second-order coherence function of Eq. (5) by the mean intensity of both detectors, resulting in

$$g^{(2)}(\tau) \propto 1 + \frac{\sin^2(N\omega_b\tau/2)}{\sin^2(\omega_b\tau/2)}. \quad (8)$$

Examining $g^{(2)}(\tau)$, it appears that as long as the relative delay $\tau = \tau_1 - \tau_2$ falls into the region between the periodic sharp correlation peaks, the intensity of the laser beam remains uncorrelated, corresponding to $g^{(2)} = 1$. The intensity of the laser beam is correlated, giving $g^{(2)} > 1$, only within these periodic, precise, and narrow time windows defined by the positions of the peaks. As we do not have a CW laser beam with such statistical nature of intensity fluctuations, a question naturally arises: Can the observed GFC be then considered as correlation of intensity fluctuations of the CW laser beam? The GFC in Eq. (8) is indeed calculated from the cross-interference term of Eq. (5), and hence the nonlocal interference picture is a more plausible explanation. Interestingly, this result matches the form of the intensity distribution of pulses in a traditional frequency comb. However, now our ghost frequency comb is a function of relative delay between the two photodetectors, τ , instead of proper time at a single detector. Note that this second-order correlation derivation provides the same result as Glauber's quantum theory of optical coherence.¹⁷

Figure 2 reports a typically observed GFC from the normalized temporal correlation measurement. In this measurement, we used two equal length delay lines before D_1 and D_2 such that $r_1 - r_2 = 0$. The zero-order ($n = 0$) GFC peak was observed at $t_1 - t_2 \simeq 0$. A least squares fitting concluded that the GFC in Fig. 2 has a period of $57\,386.064 \pm 0.001$ ns, equivalent to a beat frequency of $17\,425.8336 \pm 0.0003$ Hz. This value is well within the uncertainty of our estimated value of $17\,464.26 \pm 62.86$ Hz. The resulting comb-function has multipole periodic correlation peaks at $\omega_b\tau/2 = n\pi$, for $n = 0, \pm 1, \pm 2, \dots, \pm(N - 1)$. This can be written as

$$(t_1 - t_2)_n = \frac{1}{\nu_b} n + (r_1 - r_2)/c, \quad (9)$$

where we have used $\omega_b = 2\pi\nu_b$ and defined $(t_1 - t_2)_n$ as the measured value of $t_1 - t_2$ at the n th comb peak. The temporal width of each GFC peak, measured between neighboring zeros of the correlation function, is approximately

$$\Delta t \simeq \frac{1}{\nu_b N}. \quad (10)$$

Under perfect experimental conditions, which we define as having detectors with instantaneous response time, the temporal width of each GFC peak is calculated to be $\Delta t \simeq 116$ ps. Realistically, taking into account the relatively slow response times of the electronic devices, including the photodetectors, the measured temporal correlation will be the result of a time average. This time averaging contributes to the ringing artifacts as well as broadening of the measured correlation function, i.e., the temporal width of each GFC peak is broadened beyond the calculated 116 ps, as seen in Fig. 2(b).

The distinction between the GFC and a conventional frequency comb is clear: the GFC is recovered from the nonlocal measurement of second-order correlation (i.e., intensity correlation) of a multimode CW laser, while a conventional frequency comb is a pulsed laser, such as one that is mode locked, directly measured with intensity. Beyond

these differences, the pulse-like structure of the measured GFC is in fact strongly comparable to that of a traditional frequency comb with identical longitudinal modes present. Hence, we anticipate that the GFC could be used in many applications traditional frequency combs are currently used for. Despite their overwhelming success, the conventional frequency comb techniques have their limitations, and studies seeking improved performance or additional capabilities are being pursued.⁹ The relative advantages of the GFC will therefore depend on the specific cases, such as when a CW laser is favored over pulsed or when a nonlocal measurement is desired.

To demonstrate the unique advantage of the GFC, next, we present a possible application in nonlocal time transfer and clock synchronization, inspired by other works on optical time transfer.³⁷⁻³⁹ This simple setup follows the same general layout as the schematic setup of Fig. 1 but with the pair of detectors at arbitrary distances. In a potential large-scale use case, suppose two clocks are carried by Space Station 1 and Space Station 2. A CW laser beam in the ground laboratory is divided into two paths and directed to two photodetectors, D_1 in Space Station 1 and D_2 in Space Station 2, through two individual telescopes. The individual time history records can be brought together to the ground laboratory through a classical communication channel for comparison and subsequent correlation calculations. When the two clocks are synchronized, the joint photodetection between D_1 and D_2 will show an expected set of GFC peaks. If the clocks lose their synchronization, one can rematch the records by adjusting one of the clocks until the expected set of GFC peaks is achieved. The clocks can be adjusted and kept synchronized accordingly. A linear least squares fitting, following Eq. (9), is able to help in the nonlocal clock synchronization.

As a proof-of-concept demonstration, the results reported in Fig. 3 measure a GFC for a laboratory-based principle demonstration of nonlocal clock synchronization. In this measurement, we use 1 and 5 km fiber delay lines for D_1 and D_2 , respectively, to simulate the nonlocal condition. The optical distance between D_1 and D_2 is therefore 4 km (with some degree of uncertainty in the lengths of the fiber optic delays). Figure 3(b) is a least-squared fitting of the experimental data. The linear fitting matches Eq. (9) with high accuracy. The GFC has a period of $57\,386.066 \pm 0.001$ ns, equivalent to a beat frequency of $17\,425.8392 \pm 0.0003$ Hz. It is also noticed that the intersection of the fitting line on the $t_1 - t_2$ axis is $19\,569.025 \pm 0.004$ ns, corresponding to 3999.1195 ± 0.0008 m optical distance with the given index of refraction. As a result, such measurements from a GFC can aid in nonlocal timing-positioning or range finding as well as in clock synchronization. In both scenarios, presented in Figs. 2 and 3, the measured comb spacing is proven to be consistent. As the pulse-like structure of the frequency comb is uncovered through the measured correlation from the two independent photodetectors, it can be labeled as a "ghost" frequency comb. Additionally, the optical delay between the detectors has also been measured with high precision.

The accuracy of our measurements, characterized by the error in the least squares fitting, is on the order of picoseconds to sub-picoseconds with a data acquisition time of approximately milliseconds. This proof-of-concept demonstration is quantitatively less accurate than state-of-the-art clocks (which can reach $\sim 10^{-18}$);^{9,19,40} as such, further optimization is needed. As the presented work was done with the limited resources available at the time of the experiment, direct improvements are possible with different laser configurations

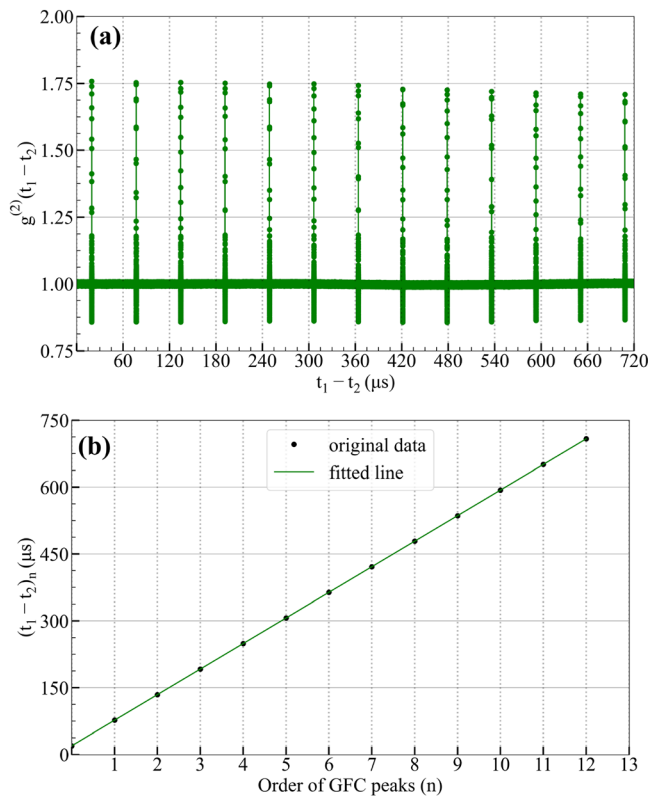


FIG. 3. (a) Measured GFC for principle demonstration of nonlocal clock synchronization. In this measurement, we used 1 and 5 km fiber delay lines for D_1 and D_2 to simulate the nonlocal condition. The optical distance between D_1 and D_2 is 4 km. The standard error of the measurement at each value of the correlation is too small to be displayed as an error bar. (b) A least squares fitting of the experimental data [an accuracy fitting of Eq. (9)]. The least squares fitting concluded that the GFC has a period of $57\,386.066 \pm 0.001$ ns, equivalent to a beat frequency of $17\,425.8392 \pm 0.0003$ Hz. Note that the intersection of the fitting line on the $t_1 - t_2$ axis is $19\,569.025 \pm 0.004$ ns, corresponding to 3999.1195 ± 0.0008 m optical distance between D_1 and D_2 .

(see the [supplementary material](#)), customizations in the detection electronics and data acquisition, and robust mechanical design. Recent progress has been made to overcome detector limitations present in optical time transfer with traditional frequency combs through linear optical sampling with an additional frequency comb offset by a known frequency.^{41,42} We believe this technique could be implemented for the GFC as well. Alongside these potential improvements, the multimode CW laser used for the GFC can offer a trade-off in terms of mobility, complexity, and cost, in line with different approaches for the realization of transportable clocks,^{43,44} given that the most accurate state-of-the-art clocks are not as flexible in terms of their design and mobility because of relatively higher size/weight and power (SWaP) requirements.^{9,19} Finally, in the context of the ongoing search for *optical* protocols as alternatives to the existing microwave-based systems for time transfer and clock synchronization,^{9,10,40} our demonstration could potentially serve as a testbed for optical time transfer and clock synchronization.

In summary, we demonstrated a nonlocal frequency-time comb in the intensity correlation of a coherent CW laser beam consisting of

a large number ($\sim 500\,000$) of longitudinal cavity modes. This result has the potential to make an important contribution to the field of precision spectroscopy, such as nonlocal time transfer or clock synchronization, and nonlocal timing-positioning. Unlike conventional frequency combs, this ghost frequency comb is uncovered through the nonlocal correlation measurement of the multi-cavity-mode CW laser beam by two distant independent photodetectors.

See the [supplementary material](#) for additional discussion on the effect of adjusting the comb spacing and related topics.

We would like to thank M. F. Locke, A. Katz, L. Yan, and M. M. Fitelson for providing us with necessary equipment and helpful suggestions. The valuable support provided by Z. Zhang for computing resources is also acknowledged. This work was partially supported by the Northrop Grumman Corporation and the Naval Air Warfare Center Aircraft Division.

AUTHOR DECLARATIONS

Conflict of Interest

The authors have no conflicts to disclose.

Author Contributions

Binod Joshi: Conceptualization (equal); Data curation (lead); Formal analysis (equal); Investigation (lead); Writing – original draft (equal). **Thomas A. Smith:** Conceptualization (equal); Formal analysis (equal); Writing – original draft (equal). **Yanhua Shih:** Conceptualization (equal); Formal analysis (equal); Supervision (lead).

DATA AVAILABILITY

The data that support the findings of this study are available from the corresponding author upon reasonable request.

REFERENCES

- J. L. Hall and T. W. Hänsch, *Opt. Lett.* **9**, 502 (1984).
- H. R. Telle, D. Meschede, and T. W. Hänsch, *Opt. Lett.* **15**, 532 (1990).
- A. Schliesser, N. Picqué, and T. Hänsch, *Nat. Photonics* **6**, 440 (2012).
- N. Picqué and T. W. Hänsch, *Nat. Photonics* **13**, 146 (2019).
- T. Fortier and E. Baumann, *Commun. Phys.* **2**, 153 (2019).
- L. Chang, S. Liu, and J. E. Bowers, *Nat. Photonics* **16**, 95 (2022).
- T. W. Hänsch, *Rev. Mod. Phys.* **78**, 1297 (2006).
- J. L. Hall, *Rev. Mod. Phys.* **78**, 1279 (2006).
- R. K. Gosalia, R. Aguinaldo, J. Green, H. Leopardi, P. Brereton, and R. Malaney, *APL Photonics* **9**, 100903 (2024).
- Z. Chen, D. Yu, G. Lu, Y. Zhang, S. Yu, B. Luo, and H. Guo, *Optica* **11**, 1268 (2024).
- H. Bergeron, L. C. Sinclair, W. C. Swann, I. Khader, K. C. Cossel, M. Cermak, J.-D. Deschênes, and N. R. Newbury, *Nat. Commun.* **10**, 1819 (2019).
- I. Coddington, W. C. Swann, L. Nenadovic, and N. R. Newbury, *Nat. Photonics* **3**, 351 (2009).
- H. Wright, J. Sun, D. McKendrick, N. Weston, and D. T. Reid, *Opt. Express* **29**, 37037 (2021).
- H. Wright, A. J. M. Nemes, N. J. Weston, and D. T. Reid, *Opt. Express* **31**, 22497 (2023).
- A. Dutt, C. Joshi, X. Ji, J. Cardenas, Y. Okawachi, K. Luke, A. L. Gaeta, and M. Lipson, *Sci. Adv.* **4**, e1701858 (2018).
- A. Einstein, B. Podolsky, and N. Rosen, *Phys. Rev.* **47**, 777 (1935).
- B. Joshi, T. A. Smith, and Y. Shih, *Phys. Rev. A* **110**, L031702 (2024).

- ¹⁸F. Riehle, *Nat. Photonics* **11**, 25 (2017).
- ¹⁹E. D. Caldwell, L. C. Sinclair, J.-D. Deschenes, F. Giorgetta, and N. R. Newbury, *APL Photonics* **9**, 016112 (2024).
- ²⁰A. Weiner, *Ultrafast Optics*, Wiley Series in Pure and Applied Optics (Wiley, 2011).
- ²¹R. H. Brown and R. Q. Twiss, *Nature* **177**, 27 (1956).
- ²²R. H. Brown and R. Q. Twiss, *Nature* **178**, 1046 (1956).
- ²³T. B. Pittman, Y. H. Shih, D. V. Strekalov, and A. V. Sergienko, *Phys. Rev. A* **52**, R3429 (1995).
- ²⁴D. V. Strekalov, A. V. Sergienko, D. N. Klyshko, and Y. H. Shih, *Phys. Rev. Lett.* **74**, 3600 (1995).
- ²⁵A. Valencia, G. Scarcelli, M. D'Angelo, and Y. Shih, *Phys. Rev. Lett.* **94**, 063601 (2005).
- ²⁶G. Scarcelli, A. Valencia, and Y. Shih, *EPL* **68**, 618 (2004).
- ²⁷G. Scarcelli, V. Berardi, and Y. Shih, *Phys. Rev. Lett.* **96**, 063602 (2006).
- ²⁸M. J. Padgett and R. W. Boyd, *Philos. Trans. R. Soc., A* **375**, 20160233 (2017).
- ²⁹P.-A. Moreau, P. A. Morris, E. Toninelli, T. Gregory, R. S. Aspden, G. Spalding, R. W. Boyd, and M. J. Padgett, *Sci. Rep.* **8**, 13183 (2018).
- ³⁰P. Janassek, S. Blumenstein, and W. Elsässer, *Phys. Rev. Appl.* **9**, 021001 (2018).
- ³¹R. J. Glauber, *Phys. Rev. Lett.* **10**, 84 (1963a).
- ³²R. J. Glauber, *Phys. Rev.* **131**, 2766 (1963b).
- ³³A. V. Burlakov, M. V. Chekhova, O. A. Karabutova, and S. P. Kulik, *Phys. Rev. A* **63**, 053801 (2001).
- ³⁴O. Kwon, Y.-S. Ra, and Y.-H. Kim, *Opt. Express* **17**, 13059 (2009).
- ³⁵D.-G. Im, Y. Kim, and Y.-H. Kim, *Opt. Express* **27**, 7593 (2019).
- ³⁶O. Svelto, *Principles of Lasers* (Springer US, 2010).
- ³⁷A. Valencia, G. Scarcelli, and Y. Shih, *Appl. Phys. Lett.* **85**, 2655 (2004).
- ³⁸R. Jozsa, D. S. Abrams, J. P. Dowling, and C. P. Williams, *Phys. Rev. Lett.* **85**, 2010 (2000).
- ³⁹V. Giovannetti, S. Lloyd, L. Maccone, and F. N. C. Wong, *Phys. Rev. Lett.* **87**, 117902 (2001).
- ⁴⁰Q. Shen, J.-Y. Guan, T. Zeng, Q.-M. Lu, L. Huang, Y. Cao, J.-P. Chen, T.-Q. Tao, J.-C. Wu, L. Hou, S.-K. Liao, J.-G. Ren, J. Yin, J.-J. Jia, H.-F. Jiang, C.-Z. Peng, Q. Zhang, and J.-W. Pan, *Optica* **8**, 471 (2021).
- ⁴¹J.-D. Deschênes, L. C. Sinclair, F. R. Giorgetta, W. C. Swann, E. Baumann, H. Bergeron, M. Cermak, I. Coddington, and N. R. Newbury, *Phys. Rev. X* **6**(2), 021016 (2016).
- ⁴²F. R. Giorgetta, W. C. Swann, L. C. Sinclair, E. Baumann, I. Coddington, and N. R. Newbury, *Nat. Photonics* **7**(6), 434–438 (2013).
- ⁴³S. B. Koller, J. Grotti, S. Vogt, A. Al-Masoudi, S. Dörscher, S. Häfner, U. Sterr, and C. Lisdat, *Phys. Rev. Lett.* **118**, 073601 (2017).
- ⁴⁴Z. L. Newman, V. Maurice, T. Drake, J. R. Stone, T. C. Briles, D. T. Spencer, C. Fredrick, Q. Li, D. Westly, B. R. Ilic, B. Shen, M.-G. Suh, K. Y. Yang, C. Johnson, D. M. S. Johnson, L. Hollberg, K. J. Vahala, K. Srinivasan, S. A. Diddams, J. Kitching, S. B. Papp, and M. T. Hummon, *Optica* **6**, 680 (2019).